Progress In Electromagnetics Research B, Vol. 54, 89–106, 2013

LOCAL OSCILLATOR UNCORRELATED PHASE NOISE ANALYSIS FOR MILLIMETER-WAVE PASSIVE IMAGER BHU-2D FREQUENCY SYNTHESIZER

Jin Zhang*, Zhiping Li, Cheng Zheng, Xianxun Yao, Baohua Yang, and Jungang Miao

School of Electronic & Information Engineering, Beihang University, Beijing, China

Abstract—In this paper, a nontrivial local oscillator uncorrelated phase noise analysis is proposed for frequency synthesizer of a passive millimeter-wave Synthetic Aperture Interferometric Radiometer (SAIR) imager BHU-2D designed for concealed weapon detections on human bodies with high imaging rates. The frequency synthesizer provides local oscillator signals for both millimeter-wave front-ends and intermediate frequency I/Q demodulators for the receivers. The influence of local oscillator uncorrelated phase noise in different offset frequency ranges on the visibility phase errors have been systematically investigated, and the corresponding system-level visibility specifications are drawn. The integrated RMS phase error has been applied to set uncorrelated phase noise requirements in the most critical offset frequency range for visibility error control. The synthesizer design is given, and measurement results have proved that the visibility phase error requirement is achieved by the PN analysis method proposed with system-level visibility error tests performed. To conclude, the phase noise effects on SAIR visibility phase errors are investigated by theory, and are properly limited by the PN requirement analysis method to ensure that the system-level visibility phase error specification is satisfied.

Received 20 May 2013, Accepted 22 August 2013, Scheduled 28 August 2013

* Corresponding author: Jin Zhang (zhangjin850224@139.com).

1. INTRODUCTION

Various techniques in the area of concealed weapon detection on human bodies have been developed and widely applied to security checks. Compared with active detection systems, such as the X-ray sensors, the passive SAIR imaging system [1] provides several advantages. It only receives rather than emitting high frequency signals and does not result in human health concerns [2]. Moreover, any concealed hazards, including non-metallic weapons, can be observed in the obtained image explicitly [3–5].

Visibility error is significant for a SAIR system and has been studied in detail by related researchers. Frequency Synthesizer (FS) provides two local oscillators (LO) for millimeter-wave (mmW) front-ends and IF IQ demodulators, and it is illustrated in this paper that LO phase noise (PN) contributes to visibility phase errors. The uncorrelated PN analysis consists of 3 key problems which are solved by this paper: 1, finding the connections between LO PN effects and the visibility phase errors by SAIR signal processing theory, and drawing the system-level visibility phase error specifications; 2, establishing proper SAIR LO PN design requirements in the frequency domain; 3, realizing FS design and check if the PN requirements and the visibility phase error requirement are reached by system-level experiments.

The arrangement of this paper is from theory to experiments. In Section 2, the system and FS are briefly reviewed, and the PN effects on visibility phase errors from FS are illustrated by system-level visibility phase error analysis. In Section 3, the PN requirement analysis method is proposed in the frequency domain. In Section 4, the FS design is realized, and the PN measurements are given; with a system-level experiment, the visibility phase error specifications are realized. The FS designed has been successfully in operation in the BHU-2D system.

2. SYSTEM-LEVEL PN IMPACTS ON VISIBILITY PHASE ERROR

A SAIR imager named BHU-2D [6] has been developed by Beihang University. It consists of a 48-element U-shape antenna array, and each receiver channel is composed of a mmW receiver [7–9] and an IF IQ demodulator. The DSP subsystem computes complex correlations between IF I/Q output pairs of all receivers simultaneously, with the results calibrated to form visibility samples, whose IFT generate the brightness temperature of the field of view (FOV). Key parameters of BHU-2D are given in Table 1, and its simplified block diagram is shown

Table 1. BHU-2D general specifications.

Parameter	Specification
Effective Distance	2.5–5 m
Range Resolution	6.5 cm@3 m
Imaging Rates	$2 \sim 20$ images/sec
Center Frequency	34 GHz
Geometry of Antenna Array	U Shape
Antenna Element Spacing	2.62 wavelength (Horizontal) 1.46 wavelength (Vertical)
Field of View (FOV)	22° (Horizontal) 40° (Vertical)
Synthetic Beamwidth	1.4° (Horizontal) 1.2° (Vertical)
Receiver Type	Dual Conversion (DSB for I/Q Demodulator)
Receiver Noise Figure	4.1 dB
Receiver Bandwidth	400 MHz
LO Frequency	32 GHz (mmW Front End) 2 GHz (I/Q Demodulator)
Power Measurement System	8 bit ADC (200 MSPS) and Auto Correlator
Calibration Method	Noise Injection (External Point Source and Background Cancellation)
Single Image Integration Time (SIIT)	$0.05\,\text{s} \sim 0.5\,\text{s}$
Visibility Real or Imaginary Part Standard Deviation Uncertainty	5% (Same Input Amplitude)

in Fig. 1 [6]. A 32 GHz mmW LO and a 2 GHz IF demodulator LO are required. Fig. 2 gives the double side-band (DSB) dual-conversion receiver structure [6].

As Ku and higher frequency multipliers are easy to be integrated in the mmW front-end, 4 GHz output is selected for FS. Both LO

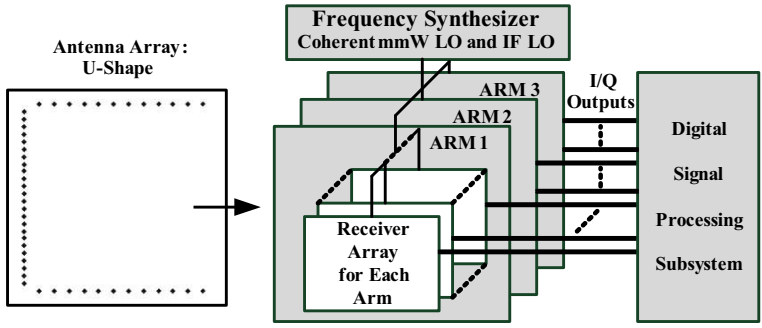

Figure 1. System configuration of BHU-2D.

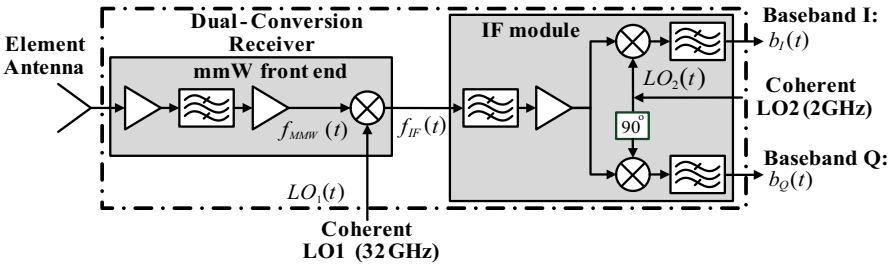

Figure 2. Dual-conversion receiver block diagram.

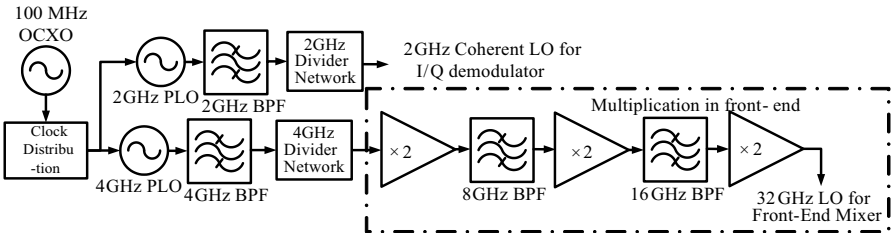

Figure 3. Preliminary FS design block diagram.

come from the same reference OCXO for coherency and low PN. Power dividers are designed at 2 and 4 GHz for lower loss. FS block diagram is shown in Fig. 3.

In Section 2, the imaging principle is briefly reviewed, and the PN effects on visibility phase errors are discussed in detail. Firstly, the uncorrelated PN effects on correlation coefficient phase errors are

shown; secondly, the standard deviation specification of the real and imaginary part of visibility are used to derive the visibility phase error standard deviation specification, to which the PN analysis and control method must be consistent.

2.1. Imaging Principle Review

The principle of SAIR is to measure the spectral components of the brightness temperature distribution in the FOV by correlating signals that are received by the antennas arranged in a plane. The correlation between a pair of received signals is [1, 6]:

$$V_{ij}(u,v) = \frac{1}{2} E\left[b_i(t) b_j^*(t)\right] \tag{1}$$

where $E[\cdot]$ is the expectation operator, and * denotes conjugated signal. $V_{ij}(u,v)$ is the correlation coefficient, which is a spatial frequency component. $b_i(t)$ and $b_j(t)$ are the signals received by the two antennas (as shown in Fig. 2), and (u,v) is the vector between the two antennas in wavelength (the baseline). Based on Van-Cittert-Zernike Theorem [10], the relationship between visibility and brightness temperature in the FOV is [6]:

$$V_{ij}(u,v) = \iint_{\xi^2+\eta^2=0}^{1} T_M(\xi,\eta)\, r_{ij}(-\tau) e^{-j2\pi(u\xi+v\eta)} d\xi d\eta \tag{2}$$

This is the integral form of the SAIR imaging principle, where $T_M(\xi,\eta)$ is modified brightness temperature which consists of the true target brightness temperature and antenna radiation patterns, and $r_{ij}(-\tau)$ is Fringe Washing Function (FWF). $\xi = \sin\theta\cos\varphi$ and $\eta = \sin\theta\sin\varphi$ are the direction cosines in spherical coordinate system. The background cancellation method for the visibility function samples could be given as:

$$V_{\text{NORM}} = \frac{V_T(u,v) - V_B(u,v)}{V_C(u,v) - V_B(u,v)} \tag{3}$$

where $V_T(u,v)$ is the target visibility, $V_B(u,v)$ the background visibility, and $V_C(u,v)$ the visibility of the calibration point source used to recover the correct imaging results. With Eq. (1) and Eq. (2), the image can be reconstructed by the inverse Fourier Transform of this pre-processed visibility of Eq. (3) [6].

By the above analysis, visibility is a key factor in SAIR imaging principle, and its errors can lead to IFT reconstruction errors, which result in distorted images. Therefore, the analysis of PN effects should be focused on their impacts on visibility phase errors.

2.2. Uncorrelated PN Effects on Visibility Phase Errors

Previous SAIR researches have given that coherent FS PN has negligible effects on visibility functions. If the PN of the two LOs of the two receiver channels are perfectly identical, their visibility is:

$$\begin{aligned} V_{ij}(u,v) &= \frac{1}{2}E\left[b_i(t)b_j^*(t)\right] = \frac{1}{2}E\left[A_{b_i(t)}A_{bj(t)}^*\right]E\left[e^{j(\emptyset_{bi}(t)-\emptyset_{bj}(t))}\right] \\ &= \frac{1}{2}E\left[A_{b_i(t)}A_{bj(t)}^*\right] \end{aligned} \tag{4}$$

where $A_{b_{i,j}(t)}$ and $\emptyset_{bi}(t)$ are the amplitude and phase of IF I/Q output signal pairs. Perfect correlated PN does not have any effect over the computed visibility, since the phase terms are cancelled in this correlation [1].

In practical SAIR receivers, different channels do produce uncorrelated PN which generates visibility errors. This fact is analyzed by system-level phase transfer modeling. Uncorrelated PN is also known as LO phase mismatch between receiver pairs. Firstly, it is assumed that phase terms of all signals are constant without PN effects. Let $f_{\mathrm{mmW}}(t)$, $\mathrm{LO}_1(t)$, $f_{\mathrm{IF}}(t)$, $\mathrm{LO}_{\mathrm{IFI}}(t)$, $\mathrm{LO}_{\mathrm{IFQ}}(t)$ be the narrow-band mmW received signal, mmW mixer LO, IF down converted signal and IF I/Q demodulator LOs, as shown in Fig. 2. They are given as:

$$f_{\mathrm{mmW}}(t) = A_{\mathrm{mmW}}\cos\left(\omega_{\mathrm{mmW}}t+\emptyset_{\mathrm{mmW}}\right) \tag{5}$$

$$\mathrm{LO}_1(t) = A_{\mathrm{LO1}}\cos\left(\omega_{\mathrm{LO1}}t+\emptyset_{\mathrm{LO1}}\right) \tag{6}$$

$$\mathrm{LO}_{\mathrm{IFI}}(t) = A_{\mathrm{LO2}}\cos\left(\omega_{\mathrm{LO2}}t+\emptyset_{\mathrm{LO2}}\right) \tag{7}$$

$$\mathrm{LO}_{\mathrm{IFQ}}(t) = A_{\mathrm{LO2}}\cos\left(\omega_{\mathrm{LO2}}t+\emptyset_{\mathrm{LO2}}+90^\circ\right) \tag{8}$$

where A and $\emptyset$ are given as the amplitude and phase terms for each signal, and subscripts LO1 and LO2 represent the mmW and IF LO. $f_{\mathrm{IF}}(t)$ and $b_i(t)$ are given as:

$$f_{\mathrm{IF}}(t) = K_1 f_{\mathrm{mmW}}(t)\mathrm{LO}_{\mathrm{mmW}}(t) \tag{9}$$

$$b_{I,Q}(t) = K_2 f_{\mathrm{IF}}(t)\mathrm{LO}_{\mathrm{IFI,\,Q}}(t) \tag{10}$$

where $K_{1,2}$ refers to the conversion loss of the mmW mixer and IF demodulator. As the mmW mixer is single side-band (SSB) and the IF I/Q demodulator is double side-band (DSB), the phase terms of $b_I(t)$ and $b_Q(t)$ can be given as:

$$\emptyset_{b_I}(t) = \emptyset_{\mathrm{mmW}}-\emptyset_{\mathrm{LO1}}\pm\emptyset_{\mathrm{LO2}} \tag{11}$$

$$\emptyset_{b_Q}(t) = \emptyset_{\mathrm{mmW}}-\emptyset_{\mathrm{LO1}}\pm\left(\emptyset_{\mathrm{LO2}}+90^\circ\right) \tag{12}$$

From Eqs. (11) and (12), the phase terms of IF I/Q demodulator output signals are constants. However, PN is always present in a realizable LO, whose phase term is:

$$\emptyset_{\mathrm{LO}}(t) = \emptyset_{\mathrm{LO}}+\emptyset_n(t) \tag{13}$$

where $\emptyset_{\mathrm{LO}}(t)$ is the phase term, $\emptyset_{\mathrm{LO}}$ is the definitive phase and $\emptyset_n(t)$ is the time-variant phase drift caused by PN. The visibility function samples can be replaced by [1, 6]:

$$\begin{aligned} V_{ij} &= \frac{1}{2}E\left[b_i(t)b_j^*(t)\right] = \frac{1}{2}E\left[A_{b_i(t)}A_{bj(t)}^*\right]E\left[e^{j(\emptyset_{bi}(t)-\emptyset_{bj}(t))}\right] \\ &= \frac{1}{2}E\left[A_{b_i(t)}A_{bj(t)}^*\right]E\left[e^{j(\mathrm{CPM}_{II,IQ}(t))}\right] \end{aligned} \tag{14}$$

A new parameter called Channel Phase Mismatch (CPM) is defined for I-I and I-Q cases as (same for QQ and QI):

$$\mathrm{CPM}_{II}(t) = \Delta\emptyset_{\mathrm{mmW}}+\Delta\emptyset_{\mathrm{LO1}}\pm\Delta\emptyset_{\mathrm{LO2}} \tag{15}$$

$$\mathrm{CPM}_{IQ}(t) = \Delta\emptyset_{\mathrm{mmW}}+\Delta\emptyset_{\mathrm{LO1}}\pm(\Delta\emptyset_{\mathrm{LO2}}-90^\circ) \tag{16}$$

where Δ refers to the phase mismatch or uncorrelated PN between receiver pairs. CPM is thus the combination of phase mismatch of mmW received signal $\Delta\emptyset_{\mathrm{mmW}}$, mmW mixer LO $\Delta\emptyset_{\mathrm{LO1}}$ and IF IQ demodulator LO phase mismatches $\Delta\emptyset_{\mathrm{LO2}}$, and $\Delta\emptyset_{\mathrm{mmW}}$ can be calibrated by point-source method [1]. $\Delta\emptyset_{\mathrm{LO1}}$ and $\Delta\emptyset_{\mathrm{LO2}}$ could be replaced by Eq. (13) as phase mismatches:

$$\Delta\emptyset_{\mathrm{LO1,2}}(t) = \Delta\emptyset_{\mathrm{LO1,2}}+\Delta\emptyset_{n1,2}(t) \tag{17}$$

where $\Delta\emptyset_{\mathrm{LO1,2}}$ is definitive and can also be calibrated to zero by point-source method [6], but $\Delta\emptyset_{n1,2}(t)$ cannot be calibrated. The visibility phase error of Eq. (14) then could be simplified to:

$$\begin{aligned} &E\left[e^{j(\mathrm{CPM}_{II,IQ}(t))}\right] = E\left[e^{j(\Delta\emptyset_{\mathrm{mmW}}+\Delta\emptyset_{\mathrm{LO1}}\pm\Delta\emptyset_{\mathrm{LO2}})}\right] \\ &\xrightarrow{\text{external point-source calibration}} E\left[e^{j(\Delta\emptyset_{n1}(t)\pm\Delta\emptyset_{n2}(t))}\right] \end{aligned} \tag{18}$$

where $\Delta\emptyset_{n1,2}(t)$ represents the uncorrelated PN in mmW LOs and IF I/Q demodulator LOs, respectively. In visibility integration, the visibility is integrated in the time domain as:

$$V_{ij} = \frac{1}{2}\langle b_i(t), b_j(t)\rangle = \frac{1}{2\tau_s}\int_0^{\tau_s} b_i(t)\times b_j^*(t)dt \tag{19}$$

Therefore, the visibility phase error caused by PN mismatch is integrated as:

$$E\left[e^{j(\Delta\emptyset_{n1}(t)+\Delta\emptyset_{n2}(t))}\right] = \frac{1}{\tau_s}\int_0^{\tau_s} e^{j(\Delta\emptyset_{n1}(t)+\Delta\emptyset_{n2}(t))}dt \tag{20}$$

where τ_s is the single image integration time (SIIT) of 0.05 s to 0.5 s. Usually, PN has a general form of phase modulation as:

$$\emptyset_n(t) = A_n\cos(\omega_m t+\psi_n) \tag{21}$$

where random amplitude A_n, offset modulation angular frequency $\omega_m = 2\pi f_m$ and random phase term ψ_n are applied in this expression. Therefore, it is concretized that τ_s and f_m are significant for uncorrelated PN requirement analysis for SAIR systems, and a clear relationship between the two should be established for PN control.

2.3. The Specification of Standard Deviation of Visibility Phase Error

As uncorrelated PN effects on visibility phase error has been verified by theory, the next problem is how to relate a system-level visibility phase error specification to verify the PN control performance qualitatively. From Table 1, it is observed that the error of real or imaginary part of visibility is defined to be within ±5% (same input amplitude for the two receiver channels), then the corresponding visibility phase error specification is found by total derivative and RMS uncertainty theories in this sub-section.

In SAIR signal processing analysis, the visibility function is also usually given in its complex form as:

$$V_{ij} = \frac{1}{2}E\left[b_i(t)b_j^*(t)\right] = V_r + jV_i \tag{22}$$

where V_r and V_i represent the real and imaginary part of the visibility sample, respectively. The phase term is:

$$\text{Phase}(V_{ij}) = \arctan\left(\frac{V_i}{V_r}\right) = f(V_i, V_r) \tag{23}$$

The total derivative of this function is used to evaluate the uncertainty of $f(V_i, V_r)$ at (x_0, y_0) as:

$$\Delta f\,(x_0,y_0) = \frac{\partial f}{\partial V_i}\,(x_0,y_0)\,\Delta V_i + \frac{\partial f}{\partial V_r}\,(x_0,y_0)\,\Delta V_r \tag{24}$$

To evaluate visibility uncertainties ΔV_i and ΔV_r, they can be replaced by the standard deviation of V_i and V_r as (under DSB receiver and I/Q demodulator) [11, 12]:

$$\Delta V_i \;=\; \sigma_i = \sqrt{\frac{1}{2B\tau_s}\left[(T_A+T_R)^2 + V_i^2 - V_r^2\right]} \tag{25}$$

$$\Delta V_r \;=\; \sigma_r = \sqrt{\frac{1}{2B\tau_s}\left[(T_A+T_R)^2 + V_r^2 - V_i^2\right]} \tag{26}$$

In SAIR applications, $T_A+T_R \gg V_r$ or V_i is always true [12], hence the above deviation could be simplified to:

$$\sigma_i = \sigma_r = \frac{1}{\sqrt{2B\tau_s}}\,(T_A+T_R) \tag{27}$$

Therefore, using the total derivative, the RMS uncertainty of $f(V_i, V_r)$ could be given as:

$$\Delta f\,(V_i, V_r)_{\mathrm{RMS}} = \sqrt{\left(\frac{\partial f}{\partial V_i}\right)^2 \times {\sigma_i}^2 + \left(\frac{\partial f}{\partial V_r}\right)^2 \times {\sigma_r}^2}$$

$$= \frac{1}{\sqrt{2B\tau_s}}(T_A + T_R)\sqrt{\left(\frac{V_r}{V_r^2 + V_i^2}\right)^2 + \left(\frac{V_i}{V_r^2 + V_i^2}\right)^2} \tag{28}$$

In a single measurement, V_i and V_r are constants, thus, the uncertainty of Phase (V_{ij}) is only related to SIIT τ_s, receiver bandwidth B, antenna and receiver temperature, T_A and T_R. Therefore, if the input two signals are in the same amplitude, which is usually the case in experimental setup, the standard deviation of Phase (V_{ij}) is $\sqrt{2}\times\sigma_{i,j}$. For the uncertainty of this deviation, it is $\sqrt{2}\times 5\%$ (7.1%), for SIIT = 0.05 s to 0.5 s. Also, the theoretical value is changed to $\frac{1}{\sqrt{B\tau_s}}$ for visibility phase error. In SAIR experiments, the $\Delta f(V_i, V_r)_{\mathrm{RMS}}$ is usually normalized by $(T_A + T_R)$, and the visibility phase error specification to verify LO PN performance could be given as:

$$\left|\Delta f(V_i, V_r)_{\mathrm{RMS,NORM}} - \frac{1}{\sqrt{B\tau_s}}\right| < \sqrt{2} \times 5\% \cong 7.1\%$$
$$(\mathrm{SIIT} = 0.05\,\mathrm{s\ to\ } 0.5\,\mathrm{s}) \tag{29}$$

To conclude, the system-level visibility phase error specification is given in Eq. (29), for which the PN control method (discussed in Section 3) must realize.

3. LO PN REQUIREMENT ANALYSIS

Based on the analysis above, the uncorrelated PN must be carefully controlled. As the structure of the first mmW mixer LO is much more complicated than IF LO, the mmW LO is the main contributor of uncorrelated PN, hence the PN analysis is mainly focused on mmW LO. This part introduces the PN requirement design method to achieve the visibility phase error specification in Eq. (29).

As PN analysis is usually performed in frequency domain, a suitable Offset Frequency Range (OFR) separation guideline is required to define PN requirements over different OFRs. This separation is setup with the extent of correlation between two receiver channels.

3.1. OFR Separation and Uncorrelated PN Requirements

From Eq. (20), the phase error expectation is performed in the time domain from 0 to τ_s. By Fourier Transform, the three OFR separations are given by relations between correlation frequency $f_s = {}^1/_{\tau_s}$ and PN offset frequency f_m:

1. $f_m \gg f_s$. This range could be interpreted as $f_m > 100 f_s$ (Far Offset Frequency Range (FOFR)). This range is far from the actual correlation region, and phase errors caused by uncorrelated PN that lead to visibility phase errors are negligible.
2. $f_m < f_s$ (Very Near Offset Frequency Range (VNOFR)). The correlations of visibility functions actually take place in this region, and uncorrelated PN could cause huge visibility phase errors. By Eq. (15), it is necessary to give rigorous limits on phase mismatch and temperature drifts as:

$$\Delta\phi_{OLi} - \Delta\phi_{OLj} < 0.1\,\text{deg} \tag{30}$$

$$\Delta\phi_{OLi} - \Delta\phi_{OLj} < 0.05\,\text{deg}/^\circ\text{C} \tag{31}$$

   where $\Delta\phi_{OLi,j}$ refers to the mmW LO phase mismatch between different receiver pairs. These requirements are more stringent than MIRAS (1 deg for phase mismatch and temperature drift), for the working LO frequency (32 GHz) is much higher than MIRAS (1.4 GHz) [13].
3. $f_s < f_m < 100 f_s$. This range is named as Middle Offset Frequency Range (MOFR). The fact that PN in this region is not flat is easily observed, and they degrade phase matches by uncorrelated PN between receiver pairs. Also, the absolute level of PN always changes sharply in this region. Therefore, stringent PN requirements are needed.

As PN(f) is always affected by random fluctuations due to power noise, and is highly IC and circuit specific, it is difficult to accurately simulate PN on every offset frequency point. Therefore, the concept of integrated RMS phase error is applied here to limit PN. This concept is previously introduced in the PN control of communication product LOs and ADC clocks [14]. As in Fig. 4, when the integrated RMS phase error is calculated, the transform from PN to this error must be performed. The MOFR frequency range is divided into N parts equal in frequency bandwidth, and A_1, A_2, ..., A_N refer to the integrated phase noise power in dBc in each Unit BandWidth (Unit-BW). These Unit-BWs may be unequal, and the integrated RMS phase error is

given as [14]:

$$A(\text{dBc}) = A_1 + A_2 + \ldots A_N \tag{32}$$

$$\text{PhEr}_{\text{RMS,DSB}}(\text{deg}) = \sqrt{2 \times 10^{A/10}} \times 180/\pi \tag{33}$$

where $\text{PHEr}_{\text{RMS, DSB}}(\text{deg})$ refers to the integrated RMS phase error, and 2 refers to DSB integration. To concretize integrated RMS error in MOFR for the 4 GHz LO, this phase error limit could be given as:

$$\text{PhEr}_{\text{RMS,4 GHz}} = \sqrt{2 \times \int_{f_s}^{100 f_s} PN(f) df} < 0.15 \,\text{deg} \tag{34}$$

where $PN(f)$ is the PN measurement results in MOFR, and df is the unit-BW used in the transform. The integrated phase error mismatch could be defined to limit uncorrelated PN effects in MOFR as:

$$\Delta\text{PhEr}_{\text{RMS,4 GHz}} < 0.05 \,\text{deg} \tag{35}$$

The above two limits are also more stringent integrated PN requirements than MIRAS (1 deg for single side-band 1.4 GHz LO) [13].

To conclude, the OFR separation is depicted in Fig. 5, and it is quite different from common Phase-Locked Oscillator (PLO) phase noise OFR separations, which are known as flicker corner frequency range (FCFR) and in or out of loop bandwidth (ILPBW or OLPBW) frequency ranges. The FS design must follow these PN requirements in three OFRs.

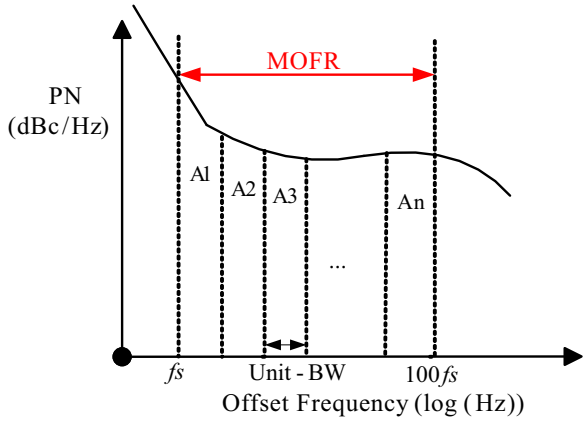

Figure 4. Integrated RMS phase error calculation in MOFR.

4. EXPERIMENT RESULTS AND DISCUSSIONS

4.1. Synthesizer Design for Uncorrelated PN Control

The design of FS PLO realized the uncorrelated PN requirements stated above. From conventional PN analysis method in PLO, the VNOFR stays well within the FCFR, and MOFR covers part of FCFR and ILPBW. Therefore, a high frequency (100 MHz) and highly stable OCXO is selected as reference, which has a very low absolute PN profile. A low PN floor PLO module and a narrow LPBW (40 kHz) are designed to realize a lower ILPBW PN for more attenuations on MOFR PN and reference spurs.

4.2. RMS Phase Error and Uncorrelated PN Test Results

As shown in Fig. 6, three output terminals of 4 GHz LO are selected for PN measurements. The PN profiles and integrated RMS errors are

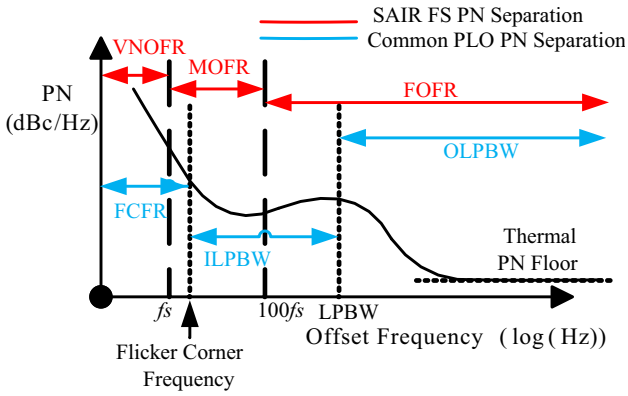

Figure 5. OFR separation for FS PN analysis (closed-loop PLO).

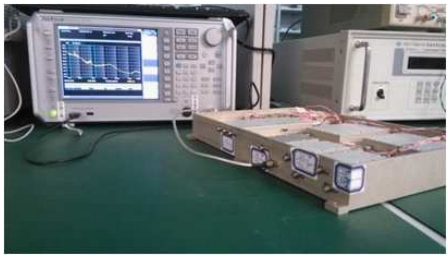

Figure 6. Phase noise measurement setup.

measured by Anritsu MS2692A (Figs. 6–7) for VNOFR, MOFR and FOFR. To decrease the negative effects of random variations of PN over a cycle of sweep time, the PN curve of each port is measured consecutively for 10 times and the averaged PN results are shown in Table 2. The PN measurements are performed in SSB, whereas integrated RMS phase errors are shown in DSB to agree with the PN requirements stated in Section 3. These results are given in Tables 4–6 for different SIITs of 0.05 s, 0.1 s and 0.5 s, with the unit-BW used for the PN to integrate RMS phase error is given in Table 3.

Table 2. Phase noise measurement results (SSB, dBc/Hz).

Offset Freq (Hz)	4 GHz-1	4 GHz-2	4 GHz-3
10	−70.16	−68.92	−69.48
100	−87.73	−86.69	−86.25
1 K	−105.07	−105.38	−105.65
10 K	−109.67	−110.20	−110.39
100 K	−119.74	−119.75	−119.67
1 M	−134.35	−134.42	−134.45

Table 3. Integrated RMS phase RMS unit-BW (Hz).

Offset Freq (Hz)	$10 \sim 100$	$100 \sim 1$ k	1 k $\sim$ 1 M
Unit Bandwidth	1	10	100

From Tables 4–6, PN mismatch requirements in VNOFR are easily reached for $\tau_s = 0.05$ s, 0.1 s and 0.5 s. The integrated RMS phase error of 4 GHz LO is limited to 0.14 deg in MOFR for the three SIITs, and a maximum phase mismatch of 0.02 deg is realized.

As observed in Fig. 7, the spikes of PN are due to 50 Hz power noise. On this PN measurement scale ($-140 \sim -60$ dBc/Hz), the three PN curves seem to be the same, especially in larger offset frequencies in FOFR. However, as shown for the uncorrelated PN or phase mismatch results in Fig. 8, PN mismatches do exist, and at some offset frequencies can reach as high as $6 \sim 7$ dB/Hz. In VNOFR and MOFR, the PN mismatches are much more severe than in FOFR, thus stringent uncorrelated PN control could never be overlooked. The previous belief that PN for every offset frequency point and for every output port is the same is only in theory and simulation, and the necessity to use integrated RMS phase error to limit uncorrelated PN in SAIR frequency synthesizer design is obviously necessary.

Table 4. Integrated RMS phase RMS results (DSB, deg), $T_s = 0.05\,\mathrm{s}$.

OFRs (Hz)	4 GHz-1	4 GHz-2	4 GHz-3
< 20 (VNOFR)	0.079	0.076	0.073
$20 \sim 2\,\mathrm{K}$ (MOFR)	0.127	0.136	0.126

Table 5. Integrated RMS phase RMS results (DSB, deg), $T_s = 0.1\,\mathrm{s}$.

OFRs (Hz)	4 GHz-1	4 GHz-2	4 GHz-3
< 10 (VNOFR)	0.056	0.058	0.055
$10 \sim 1\,\mathrm{K}$ (MOFR)	0.098	0.096	0.100

Table 6. Integrated RMS phase RMS results (DSB, deg), $T_s = 0.5\,\mathrm{s}$.

OFRs (Hz)	4 GHz-1	4 GHz-2	4 GHz-3
< 2 (VNOFR)	0.021	0.019	0.024
$2 \sim 200$ (MOFR)	0.075	0.073	0.076

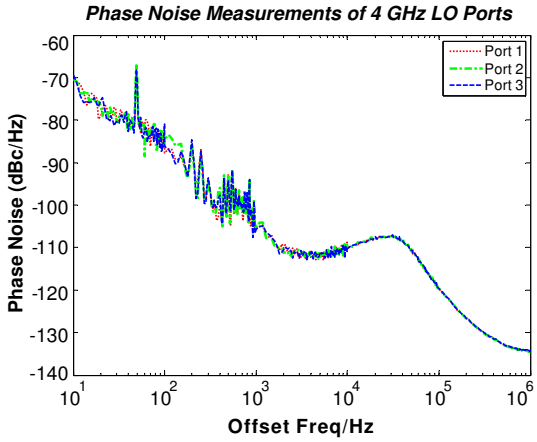

Figure 7. Phase noise measurement results.

4.3. System-level Visibility Phase Error Experiments

Based on the discussions in Section 2, an experimental verification is designed to prove that the realized PN requirements are successful in limiting visibility phase errors defined by Eq. (29). In the experiment, the standard deviations of visibility phase error compared with the theoretical value after point-source calibration are measured. To

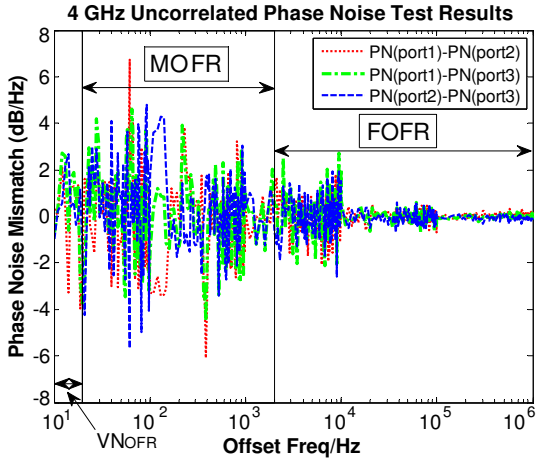

Figure 8. Phase noise mismatch measurement results.

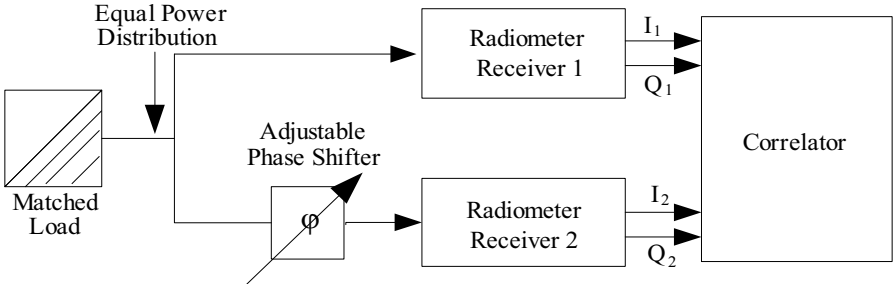

Figure 9. Phase noise mismatch measurement results.

simplify data processing, it is assumed that the power of input noise power is divided equally. The experimental block diagram is shown in Fig. 9 [15], and the test setup photo is given in Fig. 10, with two mmW front-ends, I/Q demodulators, sampling and correlators shown. The matched load generates the input noise signal and is amplified by the LNA, and then is divided equally in power by the directional coupler. Then the visibility is directly measured with the digital correlators.

In data processing, the point-source calibrations for all four correlations (I_1Q_1, I_1Q_2, I_1I_2, Q_1Q_2) are applied. The test results of the standard deviation of visibility phase errors are compared with the theoretical value ($\frac{1}{\sqrt{B\tau_s}}$) in Fig. 11. These standard deviations are measured from 10^{-3} to 6 seconds of SIIT. Inside the two dashed line, which denotes 0.05 s to 0.5 s SIIT of system requirement, the

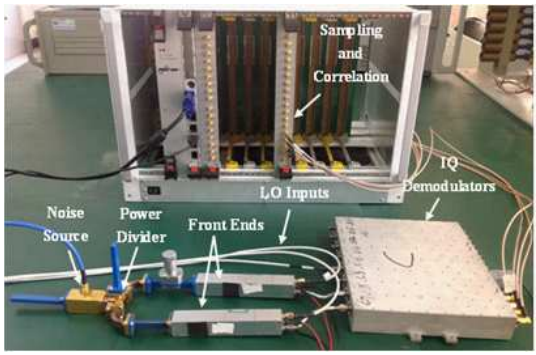

Figure 10. Visibility phase error-experiment.

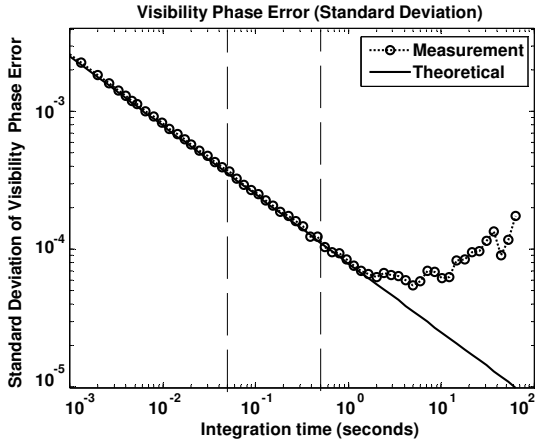

Figure 11. Normalized standard deviation of visibility phase error tests.

visibility phase errors are in good agreement with theoretical values. The maximum uncertainty of 6.2% ($< 7.1\%$) occurs at SIIT = 0.4 s. Therefore, the PN analysis method proposed is successful.

5. CONCLUSION

In this paper, uncorrelated PN effects on visibility phase errors for BHU-2D SAIR system have been investigated by SAIR signal processing theories, and the related system-level visibility phase error specifications are proposed. With a proposed PN design requirement analysis method and a proper FS design, the system-level visibility

phase error specification is achieved. The following findings are clearly observed:

1. By the theory of visibility and correlation in SAIR signal processing, the uncorrelated PN effects on correlation coefficient phase errors are shown, and the standard deviation specification of the real and imaginary part of visibility are used to derive the visibility phase error standard deviation specification in Eq. (29), with which the PN analysis and control method must be consistent.
2. By the PN design requirement analysis proposed in this paper, the correlation is transferred from time domain to frequency domain, and a set of specific uncorrelated and absolute PN control requirements are drawn. It is found that the RMS integrated phase error could be applied in defining uncorrelated and absolute PN profile requirements in VNOFR and MOFR.
3. By a nontrivial system-level experiment, the visibility phase error specification are verified to be well within the specification of Eq. (29). Therefore, the LO PN requirement analysis method is proved to be successful in limiting visibility phase errors for successful SAIR imaging system operation.

To conclude, the nontrivial PN requirement analysis method proposed by this paper has been proved to satisfy the specific SAIR systematic requirements, and the FS designed has been successfully in operation. Future optimizations on FS and PN are related to system-level improvement plans.

REFERENCES

1. Camps, A., "Application of interferometric radiometry to earth observation," Ph.D. Dissertation, Polytechnic University of Catalonia, Spain, 1996.
2. Williams, T. D. and N. M. Vaidya, "A compact, low-cost, passive mmW security scanner," *Proc. SPIE*, Vol. 5789, 109–116, May 19, 2005.
3. Notel, D., J. Huck, S. Neubert, S. Wirtz, and A. Tessmann, "A compact mmW imaging radiometer for concealed weapon detection," *Proc. IRMMW-THz*, 269–270, Cardiff, Sep. 2–9, 2007.
4. Kolinko, V. G., S. Lin, A. Shek, W. Manning, C. Martin, M. Hall, O. Kirsten, J. Moore, and D. A. Wikner, "A passive millimeter-wave imaging system for concealed weapons and explosives detection," *Proc. SPIE*, Vol. 5781, 85–92, May 19, 2005.

5. Martin, C. A. and V. G. Kolinko, "Concealed weapons detection with an improved passive millimeter-wave imager," *Proc. SPIE*, Vol. 5410, 252–259, Aug. 12, 2004.
6. Zheng, C., X. Yao, A. Hu, and J. Miao, "A passive millimeter-wave imager used for concealed weapon detection," *Progress In Electromagnetics Research B*, Vol. 46, 379–397, 2013.
7. Mehdi, G., A. Hu, and J. Miao, "Millimetre-wave all symmetric edge-coupled bandpass filter," *The 10th International Symposium on Antennas, Propagation & EM Theory*, 1271–1274, Xi'an, China, Oct. 2012.
8. Yang, B. H., G. Mehdi, A. Y. Hu, et al., "The round ended design and measurement of all symmetric edge-coupled bandpass filter," *Progress In Electromagnetics Research C*, Vol. 38, 191–203, 2013.
9. Mehdi, G., A. Hu, and J. Miao, "A highly integrated Ka-band front-end receiver," *International Journal of Computer Science Issues*, Vol. 10, Issue. 3, No. 2, 271–279, May 2013.
10. Goodman, J. W., *Statistical Optics*, 207–221, Wiley Classics Library, ed., Wiley, New York, 2000.
11. Ribo, S., "Calibration, validation and polarimetry in 2D aperture synthesis: Application to MIRAS," Ph.D Dissertation, Departament de Teoria del Senyal I Communicacions, Universitat Politecnica de Catalunya, 2005.
12. Campus, A., I. Corbella, J. Bara, and F. Torres, "Radiometric sensitivity computation in aperture synthesis interferometric radiometry," *IEEE Trans. on Geoscience and Remote Sensing*, Vol. 36, 680–685, 1998.
13. Torres, F., I. Corbella, E. Castro, et al., "Phase noise requirements in interferometric radiometers," *IGASS*, Vol. 3, 1027–1030, 2009.
14. Shinagawa, M., "Jitter analysis of high-speed sampling systems," *IEEE Journal of Solid-state Circuits*, Vol. 25, No. 1, 220–224, Feb. 1990.
15. Zheng, C., X. Yao, A. Hu, and J. Miao, "Closed form calibration of 1bit/2level correlator used for synthetic aperture interferometric radiometer," *Progress In Electromagnetics Research M*, Vol. 29, 193–205, 2013.